NOVEL MODEL BASED EMI PROCESSING FRAMEWORK

Charles Ethan Hayes, James H. McClellan, and Waymond R. Scott, Jr.

School of Electrical and Computer Engineering
Georgia Institute of Technology
Atlanta, GA, USA 30332-0250

ABSTRACT

Wideband electromagnetic induction (WEMI) sensors can be used to detect, classify, and locate metallic targets buried underground. By examining the WEMI model from a new perspective, a low-rank equivalence for the WEMI data is obtained. The low-rank physical WEMI model directly leads to a new "filterless" processing framework that differs radically from traditional approaches to WEMI processing. The new framework enables target signature recovery independent of location estimation. Processing of field data with the new filterless WEMI framework is presented to show classification results based on the low-rank target signature.

Keywords: Wideband Electromagnetic Induction, tensor, filterless, low-rank

1. INTRODUCTION

Wideband electromagnetic induction (WEMI) sensors can be used to detect, classify, and locate buried metallic targets. WEMI sensors operate by energizing eddy currents within a metallic target and then measuring the secondary magnetic fields as the target releases the energy. The traditional framework for processing measured WEMI data can be described as having three stages. The first stage uses a down-track filter that removes the self-response of the sensor.[1–3] The second stage is responsible for finding targets and recovering the targets signature.[4] The final stage locates the target and determines its orientation.[5,6] These stages are run sequentially using data recovered from the previous stages, so any errors that occur in the upstream stages affect the later stages and cause sub-optimal processing.

This work examines the physical models for the WEMI sensor and presents a mathematical approach for recovering the physical model from the sensor measurements. The approach uses a low-rank approximation of the measured data obtained via a singular value decomposition (SVD). A low-rank WEMI physical model is then obtained from the SVD which enables improved processing. The new framework is filterless and allows the detection, target signature recovery, and target location to be calculated independently and in parallel. Target orientation can then be recovered by using the target's signature and location information. Initial results for various tasks are presented to demonstrate baseline results.

2. LOW-RANK MODEL

The framework proposed in this work is directly derived from the physical model. Before introducing the framework, it is useful to review the WEMI model. The WEMI system takes a complex measurement, $\hat{M}(\omega_i, p_j)$, at each operating frequency, ω_i, and each relative target-to-sensor position, p_j. By concatenating the operating frequencies into rows and the position data into columns, a measurement matrix is created

$$\hat{\mathbf{M}}(\boldsymbol{\omega}, \mathbf{p}) = [\hat{M}(\omega_i, p_j)]_{i,j} \tag{1}$$

Further author information: (Send correspondence to C.E.H.)
C.E.H.: E-mail: chayes30@gatech.edu

where $\hat{\mathbf{M}} \in \mathfrak{C}^{N \times M}$. It is convenient to separate the real and imaginary portion of $\hat{\mathbf{M}}(\boldsymbol{\omega}, \mathbf{p})$ because it simplifies the process of extracting physical parameters that are real without a loss of information. This allows the processing to be simplified by working with a real matrix $\mathbf{M}(\boldsymbol{\omega}, \mathbf{p}) \in \mathfrak{R}^{2N \times M}$ where

$$\mathbf{M}(\boldsymbol{\omega}, \mathbf{p}) = \begin{bmatrix} \Re\{\hat{\mathbf{M}}(\boldsymbol{\omega}, \mathbf{p})\} \\ \Im\{\hat{\mathbf{M}}(\boldsymbol{\omega}, \mathbf{p})\} \end{bmatrix}. \tag{2}$$

The model for the measured data can be written as

$$\mathbf{M}(\boldsymbol{\omega}, \mathbf{p}) = \mathbf{S}(\boldsymbol{\omega}, \mathbf{p}) + \mathbf{G}(\boldsymbol{\omega}, \mathbf{p}) + \mathbf{R}(\boldsymbol{\omega}, \mathbf{p}) + \mathcal{E} \tag{3}$$

where $\mathbf{S}(\boldsymbol{\omega}, \mathbf{p})$ is the desired target response, $\mathbf{G}(\boldsymbol{\omega}, \mathbf{p})$ models the interference generated from the soil response, $\mathbf{R}(\boldsymbol{\omega}, \mathbf{p})$ is a self response of the WEMI sensor, and $\mathcal{E}$ is a Gaussian noise term where each matrix element is drawn from a $\mathcal{N}(0, \sigma^2)$ distribution. In order to understand the measurements, it is necessary to take a closer look at each of the components in (3).

The soil response has been studied previously in Ref. 7 where an empirical model for the soil response was found. The soil response is contained in a two-dimensional subspace within the operating frequency dimension that is described as

$$\hat{\boldsymbol{\Psi}}(\boldsymbol{\omega}) = \begin{bmatrix} 1 & \log(\frac{\boldsymbol{\omega}}{\omega_c}) + \frac{j\pi}{2} \end{bmatrix} \tag{4}$$

where $\hat{\boldsymbol{\Psi}}(\boldsymbol{\omega}) \in \mathfrak{C}^{N \times 2}$ and ω_c is a constant where the geometric mean of $\boldsymbol{\omega}$ can be chosen to create orthogonal basis vectors. The soil response $\mathbf{G}$ can be written as

$$\mathbf{G}(\boldsymbol{\omega}, \mathbf{p}) = \begin{bmatrix} \Re\{\hat{\boldsymbol{\Psi}}(\boldsymbol{\omega})\} \\ \Im\{\hat{\boldsymbol{\Psi}}(\boldsymbol{\omega})\} \end{bmatrix} \boldsymbol{\Xi}(\mathbf{p}) \tag{5}$$

where $\boldsymbol{\Xi}(\mathbf{p}) \in \mathfrak{R}^{2 \times M}$ is the position dependent term of $\mathbf{G}$ that is highly varying and unpredictable.

The self response $\mathbf{R}(\boldsymbol{\omega}, \mathbf{p})$ is an artifact from the transmitter coil and receiver coils of the WEMI system coupling together. This coupling is usually highly operating frequency dependent but is relatively constant in the position dimension. Because the coupling is mostly constant with only a slight drift versus time, it can be described by a constant factor along the position dimension. In practice, when the position window size is small enough, removing the DC component of the position dimension isolates the self response. However, it is useful to create a theoretical framework that allows the drift term to be removed if necessary.

The target response $\mathbf{S}(\boldsymbol{\omega}, \mathbf{p})$ contains the desired information for analysis. The proposed framework is based on the authors' new view of the target response as a low-rank matrix. The physical model for the target response can be written as the matrix product (see Appendix A):

$$\mathbf{S}(\boldsymbol{\omega}, \mathbf{p}) = \boxed{\mathbf{F}(\boldsymbol{\omega})}\ \boxed{\mathbf{T}^T}\ \boxed{\mathbf{H}(\mathbf{p})} \tag{6}$$

where $\mathbf{F}(\boldsymbol{\omega}) \in \mathfrak{R}^{2N \times K}$ is a matrix of the K relaxation frequency responses inherent to the target, $\mathbf{T} \in \mathfrak{R}^{6 \times K}$ contains the target orientation which is stored in a six-dimensional tensor for each relaxation frequency, and $\mathbf{H}(\mathbf{p}) \in \mathfrak{R}^{6 \times M}$ is the magnetic scene that describes the electromagnetic propagation when the relative position between the WEMI system and a target is $\mathbf{p}$. In order to determine the low-rank model, it is necessary to write the orientation matrix as a product

$$\mathbf{T} = \boldsymbol{\Phi}\mathbf{W} \tag{7}$$

where $\boldsymbol{\Phi} \in \mathfrak{R}^{6 \times R}$ has the R linearly independent tensors spanning $\mathbf{T}$, and $\mathbf{W} \in \mathfrak{R}^{R \times K}$ has the K weight vectors that transform $\boldsymbol{\Phi}$ into the appropriate tensors for each relaxation frequency. Inserting (7) into (6) creates

$$\mathbf{S}(\boldsymbol{\omega}, \mathbf{p}) = \boxed{\mathbf{F}(\boldsymbol{\omega})}\ \boxed{\mathbf{W}^T}\ \boxed{\boldsymbol{\Phi}^T}\ \boxed{\mathbf{H}(\mathbf{p})} \tag{8}$$

which is the low-rank signal model. The facts that $R \leq 6$, since it only needs to represent a six-dimensional space, and $R \leq K$, since it only has to create the K relaxation frequency tensors, imply that R is the rank of $\mathbf{S}$. It is important to note that $R \leq 6$ because this provides a hard limit for the maximum rank of $\mathbf{S}$ that has not been clear until now. The foregoing discussion has been a high level description of the new low-rank model; a mathematical derivation is described in Appendix A.

The final important fact about the signal model is separability of the target and position information. A processing framework is introduced below that naturally separates the frequency and positional information which allows the classification and location problems to be solved independently. A similar separation was used in Ref. 5 to separate the frequency and positional information to locate EMI targets but that separation was much more difficult to achieve and did not make use of the full rank reduction that is achieved here.

3. FRAMEWORK

The new framework exploits the low-rank model of the signal matrix and the physical model of the measurements to make the location and classification problems independent. In order to use the low-rank signal model, there are two stages. Stage one is to isolate the signal matrix in the measurements from the soil and self response. Once the signal matrix is isolated, information is extracted from the signal matrix in the second stage and used to perform detection, classification, and localization.

3.1 Isolating the signal matrix

The first stage is preprocessing that converts the measured data $\mathbf{M}$ into a smaller measured signal matrix $\mathbf{M_S}$. This framework proposes a "filterless" pre-processing scheme by using matrix projection operations. The ideal pre-processing would keep the entire signal matrix while removing the interferences, however this is not possible because the soil response, which overlaps with the desired signal in frequency $\boldsymbol{\omega}$, is not orthogonal to the signal. Even though the signal matrix $\mathbf{M_S}$ is smaller after preprocessing, it has no interference and its signal to noise ratio (SNR) is increased from the raw data because the signal has been concentrated into the smaller signal matrix.

Previous WEMI processing has used filters along the position dimension to increase SNR and isolate the self response. Instead, the "filterless" preprocessing scheme requires two orthonormal projection matrices: $\mathbf{P_R}$ and $\mathbf{P_G}$. $\mathbf{P_R}$ is a projection matrix applied to the position dimension and is responsible for isolating the self response into a low-rank subspace, leaving a useful subspace with high SNR in the position domain. For the ground response $\mathbf{P_G}$ performs the same function as $\mathbf{P_R}$ except on the operating frequency dimension, which means it creates a low-rank soil subspace and a high SNR signal subspace in the operating frequency dimension.

These projection matrices are applied to the measurements $\mathbf{M}$ as shown in Figure 1 to create a decomposition that has one submatrix for the signal, $\mathbf{M_{\bar{G}S}^{\bar{R}S}}$. The submatrix $\mathbf{M_G^R}$ contains the soil and self response and possibly has signal, $\mathbf{M_G^{\bar{R}S}}$ contains the soil response but no self response and possibly has signal, $\mathbf{M_G^{\bar{R}\mathcal{E}}}$ contains the soil response but no self response and the noise should dominate the signal, $\mathbf{M_{\bar{G}S}^R}$ contains the self response but no soil response and possibly has signal, $\mathbf{M_{\bar{G}\mathcal{E}}^R}$ contains the self response but no soil response and the noise should dominate the signal, and the remaining matrices $\mathbf{M_{\bar{G}S}^{\bar{R}S}}$, $\mathbf{M_{\bar{G}\mathcal{E}}^{\bar{R}S}}$, $\mathbf{M_{\bar{G}S}^{\bar{R}\mathcal{E}}}$, and $\mathbf{M_{\bar{G}\mathcal{E}}^{\bar{R}\mathcal{E}}}$ are all isolated from the soil and self response. It is now possible to define the measured signal matrix as

$$\mathbf{M_S} \equiv \mathbf{M_{\bar{G}S}^{\bar{R}S}} \tag{10}$$

because $\mathbf{M_{\bar{G}S}^{\bar{R}S}}$ is the only matrix that has no interference and also has improved SNR where the noise is not dominating the signal. It can also be noted that $\mathbf{M_{\bar{G}\mathcal{E}}^{\bar{R}S}}$, $\mathbf{M_{\bar{G}S}^{\bar{R}\mathcal{E}}}$, and $\mathbf{M_{\bar{G}\mathcal{E}}^{\bar{R}\mathcal{E}}}$ are ideal candidate matrices to be used for estimating the noise power σ^2. It should also be pointed out that $\mathbf{M_G^{\bar{R}S}}$ is expected to contain a large portion of the signal content. Future work will be dedicated to recovering the signal information in $\mathbf{M_G^{\bar{R}S}}$ when the soil response is weak and working to mitigate the loss of information when the soil response is stronger.

$$\mathbf{P_G}\mathbf{M}\mathbf{P}_\mathbf{R}^H =
\begin{array}{|c|c|c|}
\hline
\mathbf{M}_{\mathbf{GS}}^{\mathbf{R}} & \mathbf{M}_{\mathbf{GS}}^{\bar{\mathbf{R}}\mathbf{S}} & \mathbf{M}_{\mathbf{GS}}^{\bar{\mathbf{R}}\mathcal{E}} \\
\hline
\mathbf{M}_{\mathbf{G}\mathcal{E}}^{\mathbf{R}} & \mathbf{M}_{\mathbf{G}\mathcal{E}}^{\bar{\mathbf{R}}\mathbf{S}} & \mathbf{M}_{\mathbf{G}\mathcal{E}}^{\bar{\mathbf{R}}\mathcal{E}} \\
\hline
\mathbf{M}_{\mathbf{G}}^{\mathbf{R}} & \mathbf{M}_{\mathbf{G}}^{\bar{\mathbf{R}}\mathbf{S}} & \mathbf{M}_{\mathbf{G}}^{\bar{\mathbf{R}}\mathcal{E}} \\
\hline
\end{array}$$

Row annotations (right):
- Projected away from soil subspace / Projected into target subspace / Mostly target response
- Projected away from soil subspace / Projected away from target subspace / Mostly noise
- Projected into soil subspace / Mostly soil response with some target

Column annotations (below):
- Low-Spatial frequencies / Mostly self response
- Mid-Spatial frequencies / Mostly target response
- High-Spatial frequencies / Mostly noise

$$\tag{9}$$

Figure 1. Orthogonal projections for soil and self response applied to raw measurements $\mathbf{M}$.

3.2 Processing the signal matrix

In order to understand how to process $\mathbf{M_S}$, it is useful to investigate the optimal method to process $\mathbf{S}$. The authors' previous work[8] introduced a general method for recovering a low-rank model from a low-rank measurement matrix. This is done by first assuming a noisy version of the signal matrix

$$\hat{\mathbf{S}} = \mathbf{S} + \mathcal{E} = \mathbf{F}\mathbf{W}^T\mathbf{\Phi}^T\mathbf{H} + \mathcal{E} \tag{11}$$

that has a maximum rank of six with a noise floor defining the rest of the singular values. By taking the six largest components of the singular value decomposition (SVD) of $\hat{\mathbf{S}}$, (11) becomes

$$\hat{\mathbf{S}} = \boxed{\mathbf{U_S}}\,\boxed{\mathbf{\Sigma_S}}\,\boxed{\mathbf{V_S}^T} \quad = \quad \boxed{\mathbf{F}}\,\boxed{\mathbf{W}^T}\,\boxed{\mathbf{\Phi}^T}\,\boxed{\mathbf{H}} + \mathcal{E} \tag{12}$$

when the SNR is high. This equality leads to the recovery process of

$$\min_{\mathbf{Q_F}} \|\mathbf{U_S}\mathbf{\Sigma_S}^{\frac{1}{2}} - \mathbf{F}\mathbf{W}^T\mathbf{Q_F}\|_F \tag{13a}$$

$$\min_{\mathbf{Q_H}} \|\mathbf{V_S}\mathbf{\Sigma_S}^{\frac{1}{2}} - \mathbf{H}\mathbf{\Phi}\mathbf{Q_H}\|_F \tag{13b}$$

where $\|*\|_F$ is the Frobenius norm that minimizes the squared error of each matrix term, $\mathbf{Q_F}$ and $\mathbf{Q_H}$ are rotation and scaling matrices that are square and invertible, and the $\mathbf{\Sigma_S}^{\frac{1}{2}}$ term is included in the minimization as a weighting factor since the rank is expected to be less than six but is unknown.

Equations (13a) and (13b) show that the target characterization and localization problems have been completely separated. The $\mathbf{U_S}$ matrix now holds all of the target specific information and can be used for classification. The $\mathbf{V_S}$ matrix holds all of the location information. The only problem that is still not independent is the

tensor recovery to determine the orientation information of the target. The orientation problem can be solved using the least-squares problems of (13a) and (13b) to obtain

$$\mathbf{B_F} = \mathbf{W}^T \mathbf{Q_F} \tag{14a}$$

$$\mathbf{B_H} = \mathbf{\Phi} \mathbf{Q_H} \tag{14b}$$

which contain the tensor information. The orientation tensor for each relaxation frequency can be recovered by using $\mathbf{B_F}$ and $\mathbf{B_H}$ and the center matrix recovery technique from Ref. 8 to obtain

$$\mathbf{T} = \mathbf{B_F} \mathbf{B_H}^T. \tag{15}$$

Now that a method for processing the signal matrix has been defined, it can be directly transferred to $\mathbf{M_S}$. If the portion of the preprocessing projection matrices that create the high SNR signal subspace, which will be denoted as $\mathbf{P_R^S}$ and $\mathbf{P_G^S}$ respectively, are applied to $\mathbf{M_S}$, then it becomes

$$\mathbf{M_S} = \mathbf{P_G^S} \left[\mathbf{S} + \mathbf{G} + \mathbf{R} + \mathcal{E} \right] \mathbf{P_R^S}^H = \mathbf{P_G^S} \mathbf{S} \mathbf{P_R^S}^H + \hat{\mathcal{E}} \tag{16}$$

which has the desired form as in (11). This allows (12),(13a), and (13b) to be rewritten as

$$\mathbf{U_M} \mathbf{\Sigma_M} \mathbf{V_M} = \mathbf{P_G^S} \mathbf{F} \mathbf{W}^T \mathbf{\Phi}^T \mathbf{H}^T \mathbf{P_R^S}^H + \hat{\mathcal{E}} \tag{17a}$$

$$\min_{\mathbf{Q_F}} \| \mathbf{U_M} \mathbf{\Sigma_M}^{\frac{1}{2}} - \mathbf{P_G^S} \mathbf{F} \mathbf{W}^T \mathbf{Q_F} \|_F \tag{17b}$$

$$\min_{\mathbf{Q_H}} \| \mathbf{V_M} \mathbf{\Sigma_M}^{\frac{1}{2}} - \mathbf{P_R^S} \mathbf{H} \mathbf{\Phi} \mathbf{Q_H} \|_F \tag{17c}$$

where $\mathbf{U_M} \mathbf{\Sigma_M} \mathbf{V_M}$ are the six largest SVD terms of $\mathbf{M_S}$.

The above discussion shows how the new framework can solve the target classification and localization problems; however, it does not yet solve the general detection problem. According to Ref. 9, it is possible to create the uniformly most powerful invariant (UMPI) detector in Gaussian noise with a known covariance structure by defining a signal and noise subspace. The detection process is discussed in more detail in the authors' previous work.[3] In general, if the signal can be described as a vector $\mathbf{z}$ where the signal content is only in $\mathbf{z}_1$ and $\mathbf{z}_2$ only has noise, then the matched subspace detector (MSD) and constant false alarm rate detector (CFAR) can be written as

$$\text{MSD)} \quad \gamma = \|\mathbf{z}_1\|_2^2 \tag{18a}$$

$$\text{CFAR)} \quad \gamma = \frac{\|\mathbf{z}_1\|_2^2}{\|\mathbf{z}\|_2^2} \tag{18b}$$

where γ is the metric that is compared to a threshold to perform detection. In order for this detection theory to be used in the new framework, it is useful to point out that the Frobenius norm of a matrix is equivalent to reshaping the matrix into a vector and taking the ℓ_2 norm. This allows (18) to be rewritten as

$$\text{MSD)} \quad \gamma = \|\mathbf{Z}_1\|_F^2 \tag{19a}$$

$$\text{CFAR)} \quad \gamma = \frac{\|\mathbf{Z}_1\|_F^2}{\|\mathbf{Z}_1\|_F^2 + \|\mathbf{Z}_2\|_F^2} \tag{19b}$$

where $\mathbf{Z}_1$ is a matrix containing the signal and noise, and $\mathbf{Z}_2$ is a matrix containing only noise. With the new detection metrics of (19), it becomes clear how UMPI detection is performed in the new framework. By defining the signal matrix and a noise matrix, (19) can be directly applied to create either CFAR or MSD detection values.

In order to illustrate the full framework, Fig. 2 presents the full flow graph of the proposed framework. In the flow graph, $\mathbf{M}_\mathcal{E}$ is the noise matrix used for CFAR detection, DSRF (Discrete Spectrum of Relaxation Frequencies) is the operation to extract the target specific relaxation frequencies $\boldsymbol{\zeta}$,[4] and $\ell_{x,y,z}$ is the location of the target.
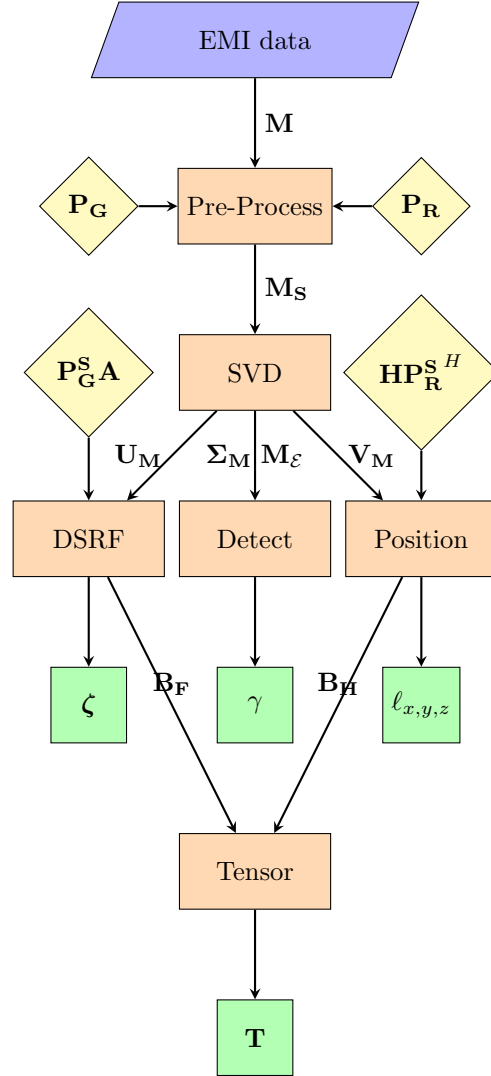
Figure 2. A flow graph of the proposed new framework.

4. PRE-PROCESSING

The high level framework was described in Sec. 3, where this section is designed to create a baseline version of the Pre-processing stage of the filterless framework. In order to create the pre-processing stage, it is necessary to create the two projection matrices: $\mathbf{P_G}$ and $\mathbf{P_R}$.

4.1 Creating $\mathbf{P_G}$

The first projection matrix that will be investigated is $\mathbf{P_G}$. In order to create $\mathbf{P_G}$, it is useful to understand the operating frequency dependent terms of $\mathbf{M}$. The soil response $\mathbf{G}$ has been previously discussed in (4). The signal matrix $\mathbf{S}$ is the only other operating frequency dependent term. Previous work[4] has defined the discrete spectrum of relaxation frequencies (DSRF), which is a dictionary matrix $\mathbf{A}$ that contains templates for the possible relaxation frequency terms ζ contained in the target. The dictionary $\mathbf{A}$ can be created by selecting a sampling of possible ζ and setting

$$A(\omega, \zeta) = \frac{j\omega/\zeta}{1 + j\omega/\zeta}. \tag{20}$$

In this work, ζ was created as 100 equally log-spaced frequencies from just below the minimum operating frequency to just above the largest operating frequency. The author's previous work[10] created a method to use $\mathbf{A}$ and the subspace spanned by $\mathbf{G}$ to create a three-portioned version of the dictionary as

$$\mathbf{A} = \mathbf{U_A} \mathbf{\Sigma_A} \mathbf{V_A}^H = \begin{bmatrix} \mathbf{U_{\bar{G}S}^A} & \mathbf{U_{\bar{G}\mathcal{E}}^A} & \mathbf{U_G^A} \end{bmatrix} \begin{bmatrix} \mathbf{\Sigma_{\bar{G}S}^A} & 0 & 0 \\ 0 & \mathbf{\Sigma_{\bar{G}\mathcal{E}}^A} & 0 \\ 0 & 0 & \mathbf{\Sigma_G^A} \end{bmatrix} \begin{bmatrix} \mathbf{V_{\bar{G}S}^A}^H \\ \mathbf{V_{\bar{G}\mathcal{E}}^A}^H \\ \mathbf{V_G^A}^H \end{bmatrix} \tag{21}$$

which contains a high SNR signal portion, noise dominated portion, and interference isolated portion of the operating frequency domain. The $\mathbf{U_A}$ matrix is the ideal projection matrix for the operating frequency domain, and so

$$\mathbf{P_G} \equiv \mathbf{U_A}. \tag{22}$$

4.2 Creating $\mathbf{P_R}$

The $\mathbf{P_G}$ matrix is similar to previous work for WEMI filters. In fact, the author's recent work of Ref. 3 can be directly used to show that the discrete cosine transform (DCT) projection matrix, $\mathcal{D}$, is a strong candidate projection matrix and this work has defined

$$\mathbf{P_R} \equiv \mathcal{D}. \tag{23}$$

The DCT matrix works well because the frequency bands can be chosen to isolate the self response, high SNR, and noise dominated subspaces. The low frequency terms contain the DC signal as well as slowly varying drift terms that isolate the self response. The high frequency terms represent position oscillations that occur too quickly for true targets, and can be used as a noise dominated subspace isolated from interference. This leaves the middle frequencies as the high SNR region where the signal content should reside. In the experiments for this work, the lowest two dimensions of the DCT were used for the self response. The noise subspace was defined as any term whose downtrack wavelength (period of the DCT term) was smaller than 5 cm. The remaining region has been shown to have most of the signal content[3] and was used as the signal subspace.

4.3 Results of Preprocessing WEMI data

Once the projection matrices were defined, the pre-processing stage was applied to data collected on a U.S. Government field site by the Georgia Tech WEMI platform.[7] The GT platform collects measurements at 21 operating frequencies, and a window length of 75 cm was chosen to process the data. This creates a measurement matrix $\mathbf{M}$ with 42 rows and roughly 150 columns. The above projection matrices were applied to $\mathbf{M}$, and a SVD was taken from the resulting $\mathbf{M_S}$. Fig. 3 shows the singular values of $\mathbf{M_S}$ calculated from the lane data. In order to empirically show that the signal matrix has a rank of six or less, a black horizontal line has been provided after the 6$^{\text{th}}$ singular value.

Note the 140 dB scale of the graph and that the strongest targets have singular values that are over 140 dB greater than the noise floor. The signal energy of all the targets is concentrated in six or fewer of the singular values; however, for the strongest targets, the signal energy in the singular values of index 7 and higher is much greater than the noise floor. For example, all the singular values of the target at 25 m in lane 4 are above the noise floor. Even though these singular values are above the noise floor, they are at least 40 dB down from the first singular value. If the sensor was perfect, only the first 6 singular values can be above the noise floor, but the sensor is not perfect. It would not take a very big sensor error to make the 7th singular value 40 dB weaker than the first singular value for a strong target. The authors believe that sensor measurement errors are the cause of the signal energy in the singular values with index of 7 and higher. The authors believe that the measurement errors are due to a combination of calibration errors and motion artifacts. These measurement errors were not apparent in previous work with this sensor, but the new framework exploits the physical model to a further degree than before which makes the measurement errors noticeable. This provides an area for further investigation in performing on-line sensor calibration by exploiting the low-rank model to further increase the fidelity of the measurements. The authors are currently using this effect to help assess the accuracy of a new sensor by using a target that is known to be of rank 1 and looking at the size of the singular vectors.

Evidence to further motivate the proposed low-rank framework is the ability to increase the WEMI platform's sensitivity. All of the lanes except lane 12 have targets that are readily apparent. The targets in lane 12 are all very difficult to detect by an EMI sensor since the targets are buried very deep and intrinsically contain weak target responses already. Even though these targets are very difficult to detect, evidence of the targets being present is seen in the graph.

5. POST-PROCESSING

The post-processing of the WEMI framework is responsible for recovering solutions to the problems about the target of interest (ToI). The three primary problems are: detection (is a ToI present?), classification (what kind of ToI is it?), and localization (where is the ToI?). Although this work does not claim to offer the optimal solutions to these questions yet, it does give baseline results using the new framework. The goal of this section is to showcase the ease of using the proposed framework to solve these problems.

5.1 Detection

The first question that must be answered is when there is a ToI present. As shown in (19), producing a MSD and CFAR detector is straight forward. In order to further simplify (19), it is useful to point out that the squared Frobenius norm of a matrix is equal to the sum of the squared singular values. This allows the signal subspace term $\|\mathbf{Z}_1\|_F^2$ to be equal to the sum of the six largest squared singular values. The signal matrix can be directly defined. For the baseline results, the remaining singular values of $\mathbf{M_S}$ were squared and summed to calculate $\|\mathbf{Z}_2\|_F^2$.

The MSD detection value for multiple lanes is shown Fig. 5. It can be seen that a threshold value of ≈ 80dB would work well as a detector for when a target is present. Fig. 5 also shows how the MSD metric varies between targets, and the threshold is strongly related to the noise floor when there is no target. The CFAR detection for the same lanes are provided in Fig. 6. A threshold of ≈ -0.025dB would work as a suitable detector for targets. The graphs in Fig. 6 reveal how the CFAR metric is normalized and has now become agnostic to signal/noise strength. When a target is present, the signal energy dominates the total power; but when a target is absent, the power is more evenly distributed through the space. Currently the noise subspace used for CFAR is dependent on the signal space, and Fig. 3 shows that signal energy is bleeding into the noise subspace for some targets. Future work will investigate using information from $\mathbf{M}_{\mathbf{G}\mathcal{E}}^{\mathbf{R}\mathbf{S}}$, $\mathbf{M}_{\mathbf{G}\mathcal{E}}^{\bar{\mathbf{R}}\mathcal{E}}$, and $\mathbf{M}_{\mathbf{G}\mathbf{S}}^{\bar{\mathbf{R}}\mathcal{E}}$ to more accurately estimate the noise subspace and improve CFAR. To compare the proposed detectors against alternative options, Ref. 3 presented these as the "filterless" detectors and showed that it outperformed all alternatives presented.

5.2 Classification

Once the ToI has been detected, the next question is to determine what type of ToI is present. This is useful to automatically determine if the target is worth further examination or is metallic debris. According to (17b), all of the target specific information is contained in $\mathbf{U_M}$. In order for classification to perform well, the targets'
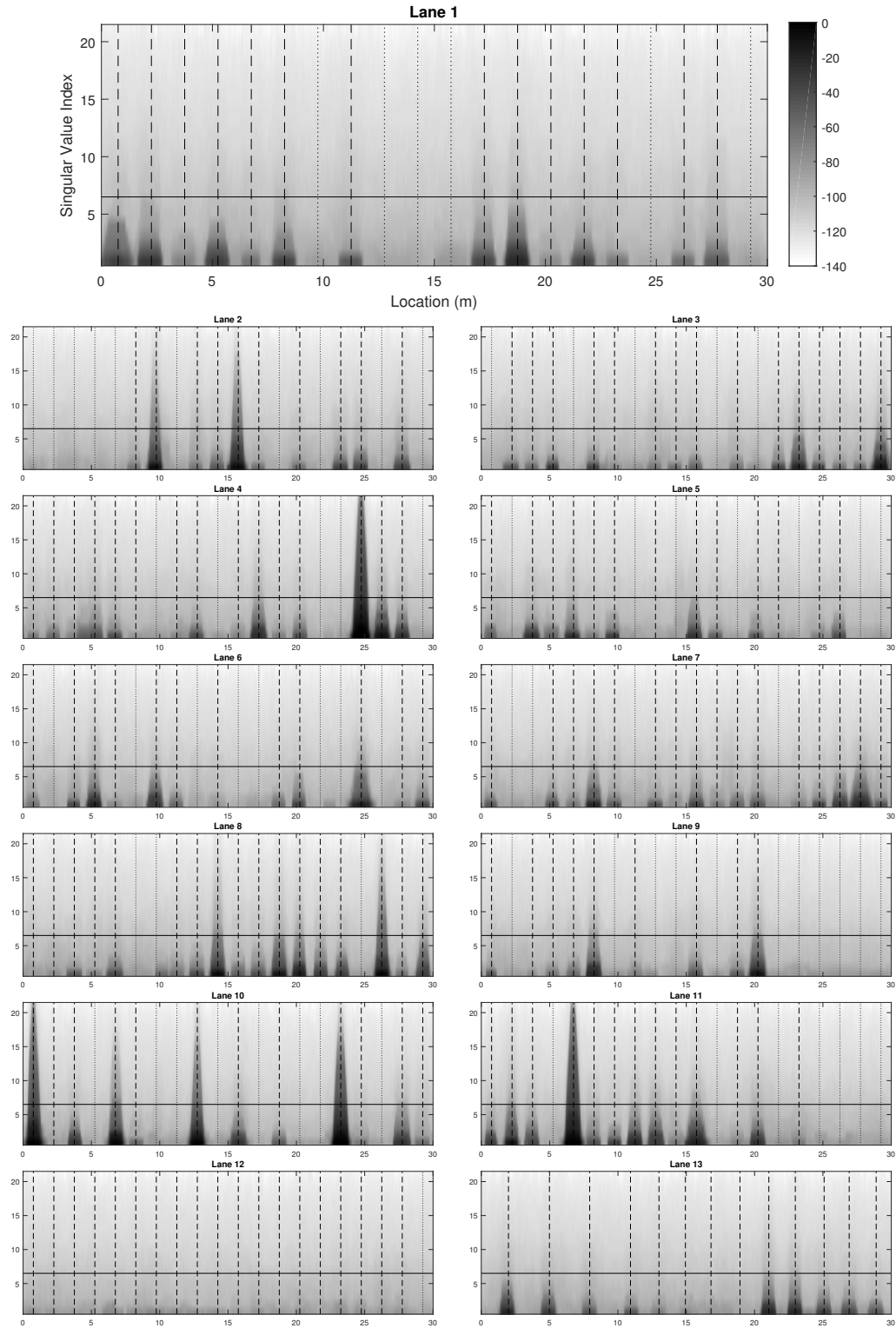
Figure 3. Singular values of signal matrix throughout the lane data. The horizontal line separates the largest 6 singular values. The dashed vertical lines indicate targets of interest and the dotted vertical lines indicate blank locations with no target. All axes and the color-scale correspond to the initial lane.
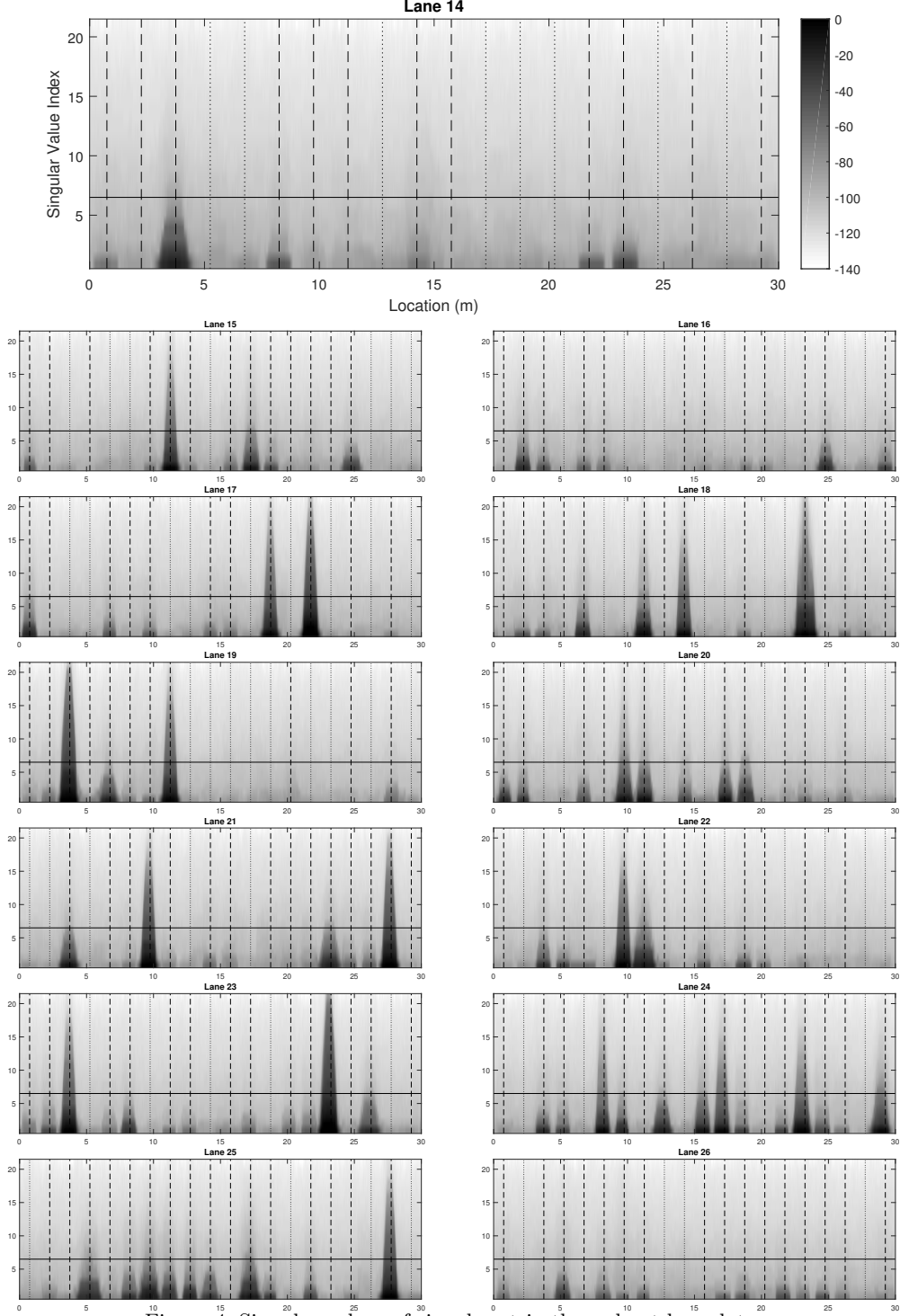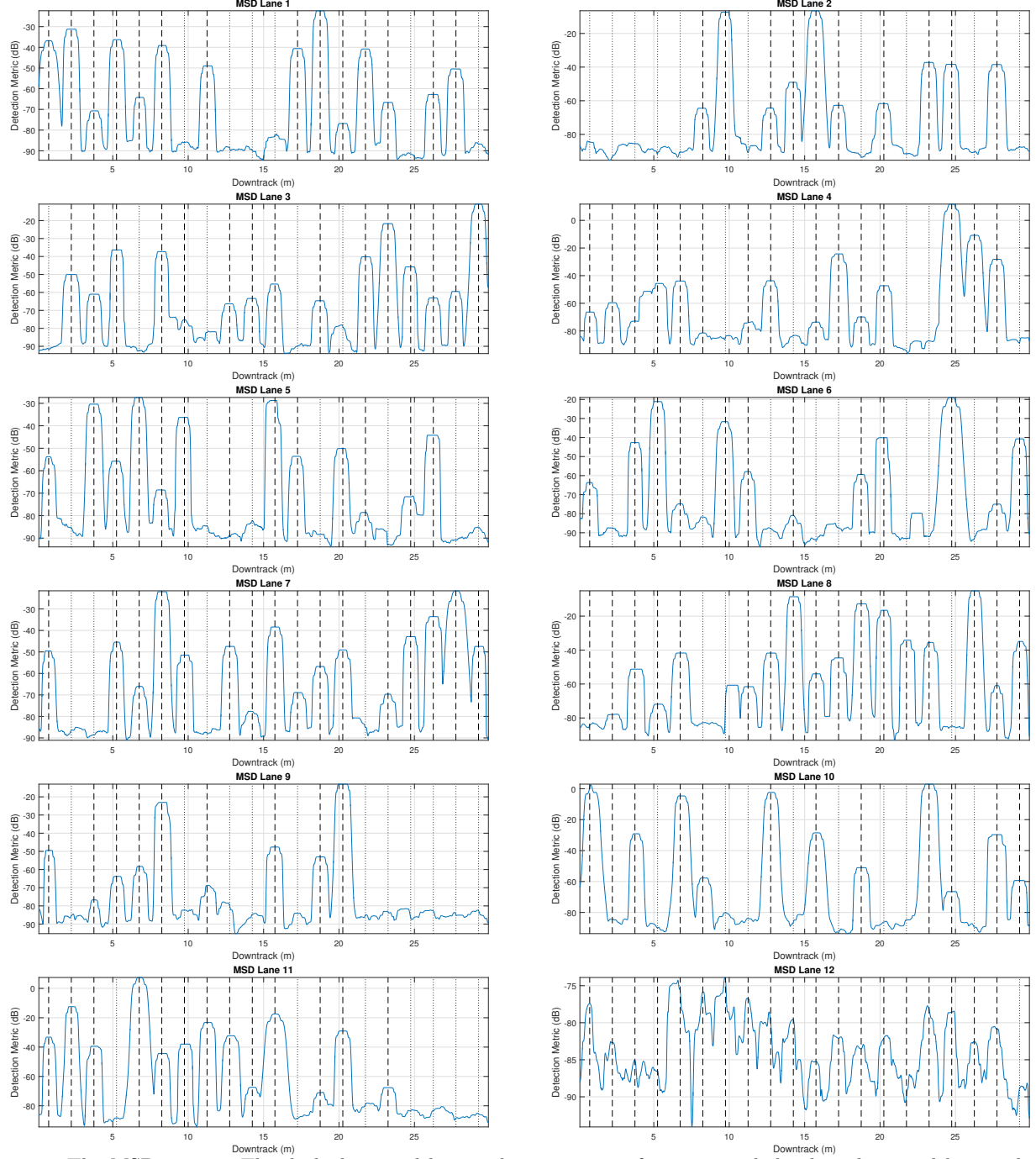
Figure 4. Singular values of signal matrix throughout lane data.

response must be repeatable. In order to illustrate the repeatability, Fig. 7–12 show the singular vectors of $\mathbf{U_M}$ for six ToIs along with their singular values. These graphs show that the singular vectors associated with singular values above the noise floor are highly repeatable between the same targets.

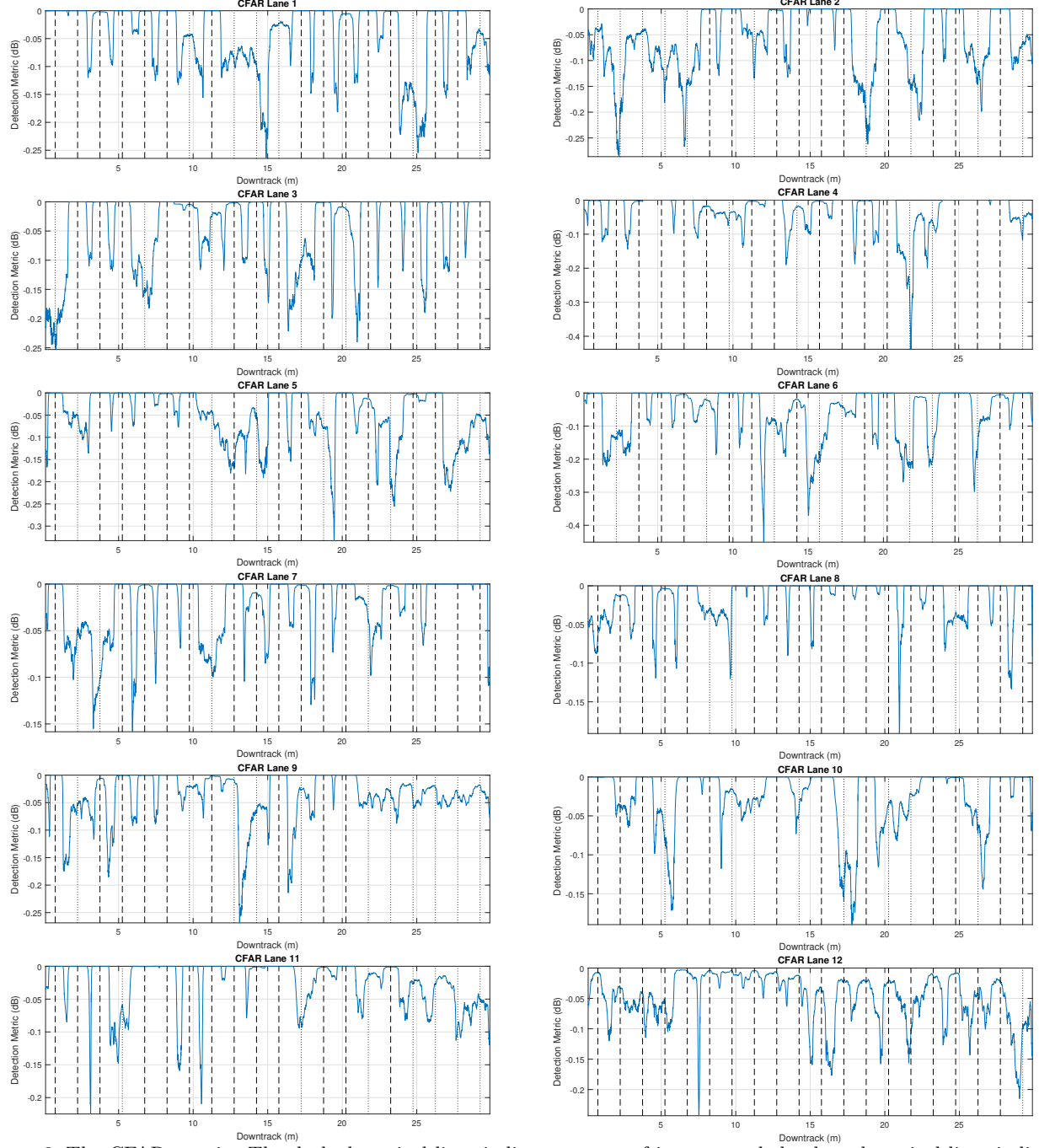In order to classify between targets, the targets must have repeatable responses that are also separable. To

Figure 5. The MSD metric. The dashed vertical lines indicate targets of interest and the dotted vertical lines indicate blank locations with no target.

test the separability of targets, a distance matrix was created between the targets and is presented in Fig. 13. The distance was calculated as the ℓ_2 norm of the difference between the largest singular vectors. The targets were organized such that the similar targets create block diagonal distance matrices. The similar targets are sorted by depth within each cluster such that the deepest target is in the top right corner of each block diagonal matrix. This was done to show the deterioration of separability from poor SNR, as the target becomes weaker when it is farther away and thus reduces the SNR. It is evident in Fig. 13 that the targets are highly separable.

Figure 6. The CFAR metric. The dashed vertical lines indicate targets of interest and the dotted vertical lines indicate blank locations with no target.

Fig. 13 provides promising baseline results for using $\mathbf{U_M}$ directly to classify targets. Future work will investigate how to better leverage the information in $\mathbf{U_M}$ for classification, as fig. 7 - 12 make it evident that there is still information to exploit in classification outside of the largest singular vector.

The DSRF has been used previously to classify targets as it extracts the unique relaxation frequencies of targets. Even though the new framework has proposed using $\mathbf{U_M}$ directly to classify targets, there is still interest in finding the relaxation frequencies. This knowledge will be necessary for recovering the tensor amplitudes and

Figure 7. The six largest singular vectors from ToI 1.

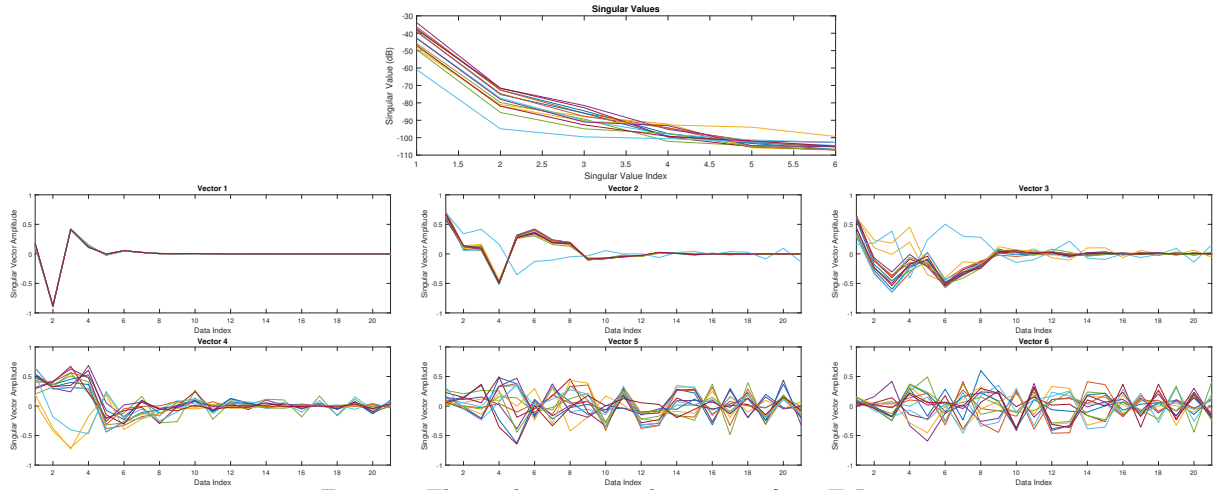Figure 8. The six largest singular vectors from ToI 2.

Figure 9. The six largest singular vectors from ToI 3.

determining orientation. Future work will investigate recovering the DSRF from $\mathbf{U_M}$.
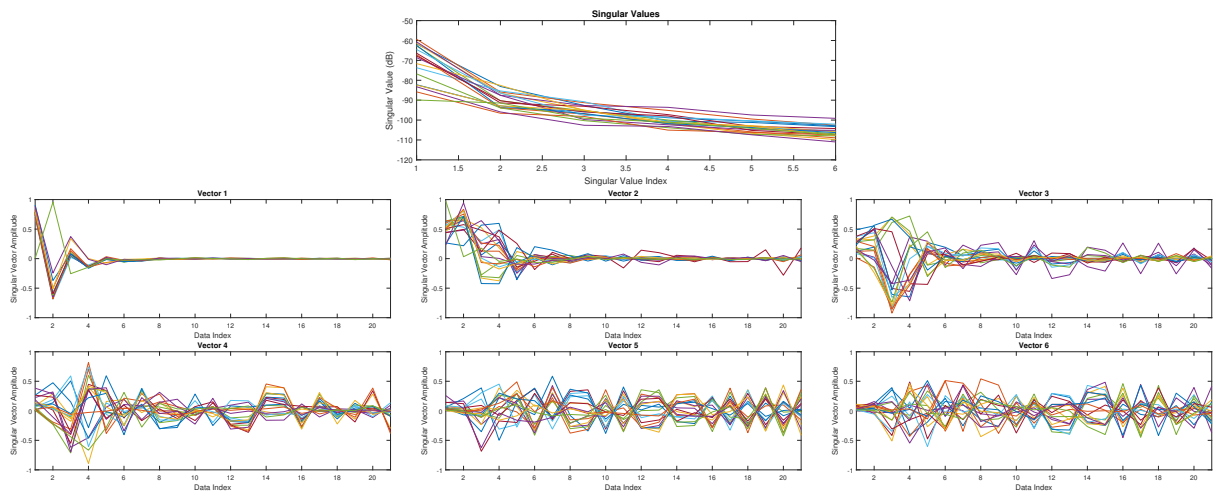
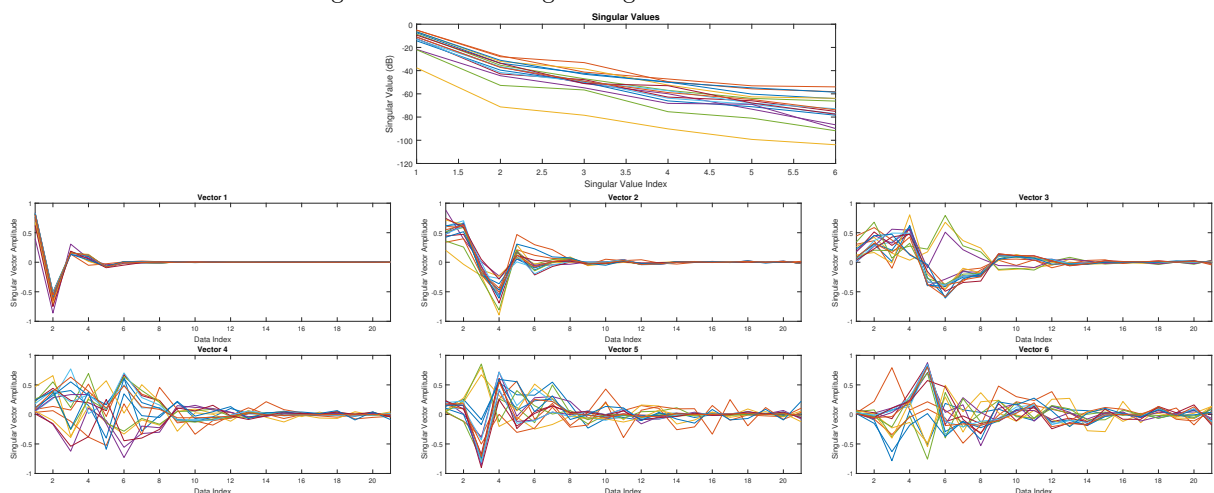Figure 10. The six largest singular vectors from ToI 14.

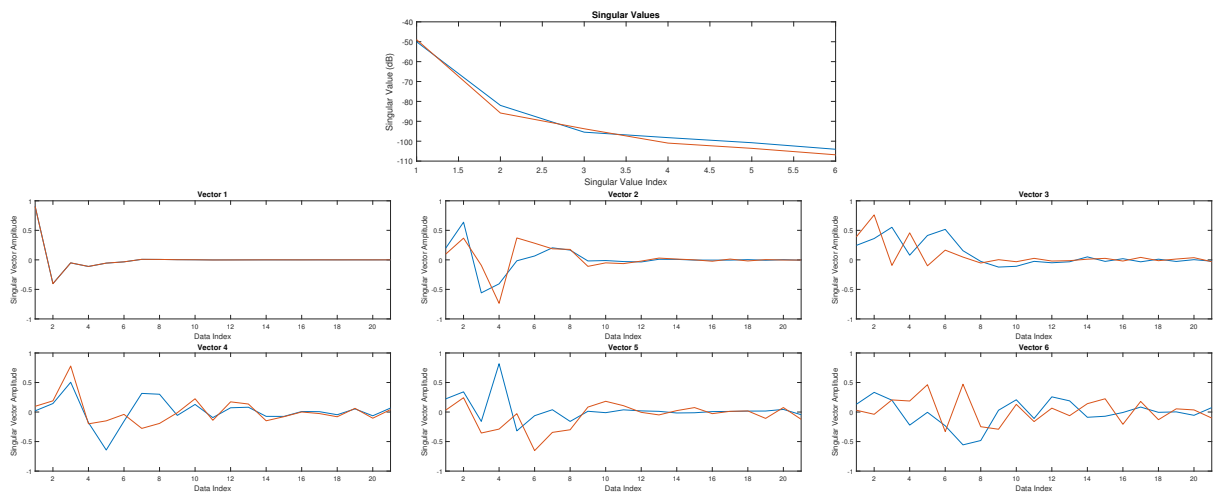Figure 11. The six largest singular vectors from ToI 24.

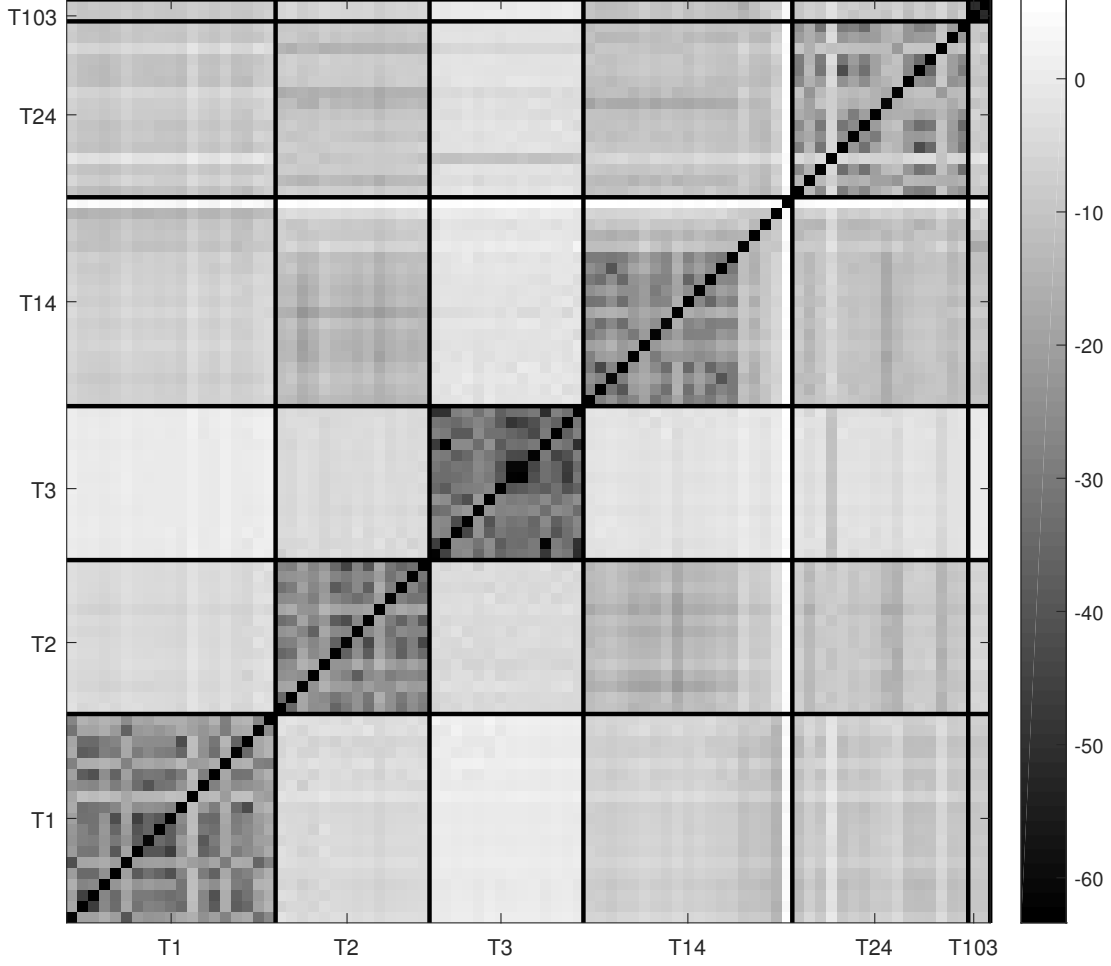Figure 12. The six largest singular vectors from ToI 103.

Figure 13. A distance matrix between some of the ToIs in the data. These distances were calculated from the Euclidean distance between the largest target singular vectors.

5.3 Localization

Once the target has been detected and classified as a desired ToI, the final question is how to locate it. The location information of the target is known to reside within $\mathbf{V_M}$ from (17c). Ref. 8 introduces a method of recovering the target location by choosing from hypothesized locations. For each hypothesized location, a magnetic scene matrix $\mathbf{H}_i$ can be created by simulating how the electromagnetic fields propagated. The correct location can then be selected by choosing the position that minimizes

$$\min_{\mathbf{H}_i, \mathbf{B}_{\mathbf{H}_i}} \|\mathbf{V_M} \mathbf{\Sigma_M}^{\frac{1}{2}} - \mathbf{P_R^S} \mathbf{H}_i \mathbf{B}_{\mathbf{H}_i}\|_F \tag{24}$$

where a $\mathbf{B_H}$ is solved for each location using least squares, and the magnetic scene model $\mathbf{H}_i$ that produces the minimum residual error is selected as the most likely position.

This work forgoes presenting localization results and refers the reader to Ref 11 where the WEMI localization problem is investigated in detail, including the proposed method.

APPENDIX A. LOW RANK MODEL MATH

The signal model for a target at a measurement frequency and relative position can be written as

$$\mathbf{S}(\omega, p) = \mathbf{h}_R(p)^T \mathbf{T}(\omega)\mathbf{h}_T(p) = \begin{bmatrix} h_{RX} \\ h_{RY} \\ h_{RZ} \end{bmatrix}^T \begin{bmatrix} t_{XX} & t_{XY} & t_{XZ} \\ t_{YX} & t_{YY} & t_{YZ} \\ t_{ZX} & t_{ZY} & t_{ZZ} \end{bmatrix} \begin{bmatrix} h_{TX} \\ h_{TY} \\ h_{TZ} \end{bmatrix} \tag{25}$$

using reciprocity[12] where $\mathbf{h}_R$ is the magnetic scene for the WEMI receiver, $\mathbf{h}_T$ is the magnetic scene for the WEMI transmitter, $\mathbf{T}$ is the target specific tensor, and allowing reciprocity constants to be incorporated into the $\mathbf{h}_*$ terms. By using the fact that $\mathbf{T}$ is symmetric, reshaping the tensor, and combining the magnetic scenes, the model can be rewritten as

$$\mathbf{S}(\omega, p) = \mathbf{h}_R(p)^T \mathbf{T}(\omega)\mathbf{h}_T(p) = \mathbf{t}(\omega)^T \mathbf{h}_A(p) = \begin{bmatrix} t_{XX} \\ t_{YY} \\ t_{ZZ} \\ t_{XY} \\ t_{XZ} \\ t_{YZ} \end{bmatrix}^T \begin{bmatrix} h_{RX}h_{TX} \\ h_{RY}h_{TY} \\ h_{RZ}h_{TZ} \\ h_{RX}h_{TY} + h_{RY}h_{TX} \\ h_{RX}h_{TZ} + h_{RZ}h_{TX} \\ h_{RZ}h_{TY} + h_{RY}h_{TZ} \end{bmatrix} \tag{26}$$

where the bilinear model has been converted into an inner product. Using the sum of relaxations model for the target polarizability,[13] the tensor amplitude can be modeled as

$$\mathbf{t}(\omega) = \alpha_0 \hat{\mathbf{t}}_0 - \sum_k \alpha_k \frac{j\omega/\zeta_k}{1 + j\omega/\zeta_k} \hat{\mathbf{t}}_k = \sum_k \alpha_k f_k(\omega)\hat{\mathbf{t}}_k \tag{27}$$

where α_k is the relaxation amplitude, ζ_k is the relaxation frequency, f_k is the DSRF term, and $\hat{\mathbf{t}}_k$ is the relaxation tensor that is no longer operating frequency dependent. The low-rank model is obtained by inserting (27) into the inner product model of (26) to create the signal model as

$$\mathbf{S}(\omega, p) = \sum_k \alpha_k f_k(\omega)\hat{\mathbf{t}}_k^T \mathbf{h}_A(p). \tag{28}$$

When the single measurement is expanded into a measurement matrix by stacking measurement frequencies and concatenating locations, the signal matrix becomes

$$\mathbf{S}(\omega, p) = \mathbf{F}\mathbf{T}^T \mathbf{H} \tag{29}$$

where the summation was converted into a matrix operation and $\mathbf{T}$ holds the orientation tensor as well as the relaxation amplitude, which can be called a "tensor amplitude". The model of (29) provides the maximum rank as six, which shows that the signal is indeed a low rank matrix. In order to predict an even smaller matrix, it is possible to show that the space spanned by the $\hat{\mathbf{t}}_k$ terms can be represented by an orthogonal basis set $\mathbf{\Phi}$ that is a subspace of the six dimensional space. If each $\hat{\mathbf{t}}_k$ is then described as a weighted sum of $\mathbf{\Phi}$, then it leads to the final low rank model

$$\mathbf{S}(\omega, p) = \mathbf{F}\mathbf{W}^T \mathbf{\Phi}^T \mathbf{H} \tag{30}$$

where $\mathbf{W}$ contains the weights for each $\hat{\mathbf{t}}_k$.

ACKNOWLEDGMENTS

REFERENCES

[1] Overton, G. and Moreland, C., [*Inside the Metal Detector*], Geotech (2012).

[2] Bruschini, C., *A Multidisciplinary Analysis of Frequency Domain Metal Detectors for Humanitarian Demining*, PhD thesis, Vrije Universiteit Brussel (2002).

[3] Hayes, C. E., McClellan, J. H., Scott Jr., W. R., and Kerr, A. J., "Improved electromagnetic induction processing with novel adaptive matched filter and matched subspace detection," *Proc. SPIE* **9823**, 98230E–98230E–14 (2016).

[4] Wei, M. H., Scott Jr., W. R., and McClellan, J., "Robust estimation of the discrete spectrum of relaxations for electromagnetic induction responses," *IEEE Transactions on Geoscience and Remote Sensing* **48**, 1169–1179 (March 2010).

[5] Krueger, K., Scott Jr., W. R., and McClellan, J. H., "Location and orientation estimation of buried targets using electromagnetic induction sensors," *Proc. SPIE* **8357**, 83570D–83570D–12 (2012).

[6] Oezdemir, M., Miller, E. L., and Norton, S., "Localization and characterization of buried objects from multifrequency array inductive data," *Proc. SPIE* **3710**, 26–36 (1999).

[7] Scott Jr., W. R., Larson, G. D., Hayes, C. E., and McClellan, J. H., "Experimental detection and discrimination of buried targets using an improved broadband CW electromagnetic induction sensor," *Proc. SPIE* **9072**, 90720C–90720C–15 (2014).

[8] Hayes, C. E., McClellan, J. H., and Scott Jr., W. R., "Low-rank physical model recovery from low-rank signal approximation," *IEEE International Conference on Acoustics, Speech, and Signal Processing (ICASSP)* (2017).

[9] Scharf, L. L. and Friedlander, B., "Matched subspace detectors," *IEEE Transactions on Signal Processing* **42**(8), 2146–2157 (1994).

[10] Hayes, C. E., McClellan, J. H., and Scott Jr., W. R., "Sparse recovery using an SVD approach to interference removal and parameter estimation," *IEEE Signal Processing & SP Education Workshop* , 202–207 (2015).

[11] Kerr, A. J., Scott Jr., W. R., Hayes, C. E., and McClellan, J. H., "Target location estimation for single channel electromagnetic induction data," *Proc. SPIE* (2017).

[12] Scott Jr., W. R. and Larson, G. D., "Modeling the measured EM induction response of targets as a sum of dipole terms each with a discrete relaxation frequency," *IEEE International Geoscience and Remote Sensing Symposium (IGARSS)* , 4188–4191 (July 2010).

[13] Baum, C. E., "Low-frequency near-field magnetic scattering from highly, but not perfectly, conducting bodies," in [*Detection and identification of visually obscured targets*], ch. 6, 163–218, CRC Press (1998).